Automatic Multimodal 2D/3D Breast Image Registration using Biomechanical FEM Models and Intensity-Based Optimization

T. Hopp[a,*], M. Dietzel[b], P. A. Baltzer[c], P. Kreisel[d], W. A. Kaiser[d], H. Gemmeke[a], N. V. Ruiter[a]

[a] *Karlsruhe Institute of Technology, Institute for Data Processing and Electronics*[1]
[b] *University of Erlangen-Nürnberg, Department of Neuroradiology*[2]
[c] *Medical University Vienna, Department of Radiology*[3]
[d] *University Hospital Jena, Department of Radiology*[4]

Abstract

Due to their different physical origin, X-ray mammography and Magnetic Resonance Imaging (MRI) provide complementary diagnostic information. However, the correlation of their images is challenging due to differences in dimensionality, patient positioning and compression state of the breast. Our automated registration takes over part of the correlation task. The registration method is based on a biomechanical Finite Element Model, which is used to simulate mammographic compression. The deformed MRI volume can be compared directly with the corresponding mammogram. The registration accuracy is determined by a number of patient-specific parameters.

* *Phone:* +49 721 / 608-2-5990, *Fax:* +49 721 / 608-2-5594 (T. Hopp)
Email address: torsten.hopp@kit.edu (T. Hopp)
URL: http://www.ipe.kit.edu (T. Hopp)
[1] Hermann-v.Helmholtz-Platz 1, 76344 Eggenstein-Leopoldshafen, Germany
[2] Schwabachanlage 6, 91054 Erlangen, Germany
[3] Währinger Gürtel 18-20, 1090 Vienna, Austria
[4] Erlanger Allee 101, 07747 Jena, Germany

Preprint submitted to Medical Image Analysis

We optimize these parameters – e.g. breast rotation – using image similarity measures. The method was evaluated on 79 datasets from clinical routine. The mean target registration error was 13.2 mm in a fully automated setting. On basis of our results, we conclude that a completely automated registration of volume images with 2D mammograms is feasible. The registration accuracy is within the clinically relevant range and thus beneficial for multimodal diagnosis.

Keywords: Multimodal Registration, Breast Imaging, Finite Element Method, Biomechanical Models, Magnetic Resonance Imaging, X-ray Mammography

---

1. Introduction

It is widely known that breast cancer is the most common cancer among women in both the developed and developing world (Fischer et al., 2007). Approximately 230,400 new cases of invasive breast cancer and additional 57,600 cases of in situ breast cancer were diagnosed in the US in 2011. In the US alone, almost 40,000 women are expected to die from breast cancer every year. Only lung cancer causes more cancer deaths in women (American Cancer Society, 2011). Mortality depends on the presence of metastases. Detection of breast cancer in an early state, i.e. at smaller size, is essential for an effective treatment since the likelihood of metastases is correlated to the size of the tumor (Sivaramakrishna and Gordon, 1997).

Medical imaging is fundamental for early diagnosis. Currently, X-ray mammography is the established screening method (Schulz-Wendtland et al., 2009). It provides a high resolution projection image of the breast, is af-

fordable and broadly available. Today full-field digital mammography has become the standard technique. Overall it shows a sensitivity of 45% to 90% respectively a specificity of 85% to 99% depending on the conducted study and is able to visualize microcalcifications. However, X-ray frequently provides poor contrast for tumors located within glandular tissue due to superimposition of different tissue. This causes a problem to women with dense breasts and the sensitivity of X-ray mammography in such cases is limited (Pisano et al., 2008).

Dynamic contrast-enhanced magnetic resonance imaging (DCE-MRI) plays an increasing role in breast imaging. It offers high contrast for soft tissue and high diagnostic accuracy (DeMartini and Lehman, 2008). Contrast agents are used to visualize lesion vasculature that is typically increased in malignant neoplasms. The evaluation of the contrast kinetics at specific time points before and after injection allows semi-quantitative tissue characterization. The information can be used to assist radiologists in their diagnosis (Kaiser and Zeitler, 1989; Baltzer et al., 2009). In contrast to X-ray mammography, the patient is not exposed to radiation. DCE-MRI has the highest sensitivity for detection of breast cancer (Houssami et al., 2008; Warner et al., 2008). Yet, the specificity is discussed controversially. Furthermore MRI is more expensive and not as widespread as X-ray mammography (Kaiser et al., 2000).

Due to their different physical origin, X-ray mammography and DCE-MRI are likely to provide complementary diagnostic information. Thus, both modalities are often read in combination for definite diagnosis. However, the combined reading of X-ray mammograms and DCE-MRI requires a lot of ex-

perience for a number of reasons. Images differ in dimensionality, patient positioning and compression state of the breast. While the mammograms show only a two-dimensional projection of the compressed breast, MRI provides three-dimensional images by acquiring multiple slice images of the breast freely hanging in prone position. As a result of the different physical origin, tissue is imaged differently in both modalities. Image registration may help to localize structures in the alternative modality and hence assist radiologists in multimodal diagnosis.

The registration of X-ray mammograms and MRI volumes is a complex task. Only few approaches have been published: Behrenbruch et al. (2003) used the breast boundary and internal landmarks for the deformation of X-ray mammograms to register them with projection images of MRI volumes. Similar to this work, Martí et al. (2004) used internal landmarks to register X-ray mammograms and MRI projection images. Both approaches did not consider the complex deformation of structures during mammographic compression. The fact that a lesion has to be visible in both modalities limits the clinical applicability for multimodal diagnosis. Mertzanidou et al. (2010) published an intensity based approach to register X-ray mammograms and MRI volumes using 3D affine transformations. However, no clinical datasets were used to account for the accuracy of this approach. The same authors used an ellipsoidal breast model and biomechanical compression simulation for registration (Mertzanidou et al., 2011). The mean registration error for ten clinical datasets and MRI to craniocaudal mammogram registration was reported to be 19.4 mm for the affine approach and 12.7 mm using the ellipsoidal breast model. Recently a study with a considerably larger number

of datasets (49 patients) was presented, achieving a median registration error of 13.1 mm (Mertzanidou et al., 2012). Rajagopal et al. (2010) used a similar technique as we applied in previous work (e.g. Ruiter et al. (2006)) to localize microcalcifications in MRI volumes by registering images using the biomechanical model of Chung et al. (2008). However the accuracy of their approach was not quantified. More recently, the same group applied the biomechanical model to the registration of X-ray mammograms and MRI volumes using four clinical datasets (Reynolds et al., 2011). Yet, several manual steps had to be carried out but the registration accuracy was still not quantified. Lee et al. (2011) recently accounted for the registration error using one dataset. By several optimizations of mammographic plate positioning, the registration error could be reduced from 16.4 mm to 3.1 mm.

In earlier work (Ruiter et al., 2006) our group developed a method for the registration of X-ray mammograms and MRI volumes. During mammography the breast is squeezed between two plates resulting in a compression of up to 50 %. The deformed breast is only depicted by a two-dimensional projection. The individual three-dimensional deformation cannot be obtained from these images. The registration method presented in this earlier work overcomes the challenge by simulating the compression applied to the breast during mammography to achieve a configuration of the MRI volume that is comparable to the mammogram. The compression simulation is carried out using a patient-specific biomechanical model. As most other biomechanical models used in medical image registration, the model is based on the Finite Element Method (FEM) since this simulation method can achieve very accurate results (Ferrant et al., 2001).

The registration method was tested with six clinical datasets and reached promising results with a mean registration error of 4.3 mm (Standard Deviation (SD): 1 mm) (Ruiter et al., 2006). Yet, the large variability of clinical datasets, e.g. rotations caused by breast rolling during mammographic compression or patient positioning during MRI examination, has not been considered in this method until now. The variability results in a lower registration accuracy in a clinical setting. Furthermore, manual steps have to be eliminated for clinical application to obtain a reproducible method. A more patient-specific automated registration is expected to deal with a larger variety of datasets and providing reasonable registration accuracy.

In this paper, we present our now completely automated registration method using an intensity-based optimization of a FEM-driven registration to deal with the patient-specific variability of clinical datasets. The method was tested with a considerably higher number of datasets (79) than any other FEM-based mammography to MRI registration.

2. Methods

The general idea of the registration method is mimicking the compression applied to the breast during X-ray mammography by a FEM simulation. The workflow showing all involved processing steps is illustrated in Figure 1. First images have to be preprocessed. Afterwards the model-based registration is carried out. Image similarity is calculated and the registration parameters are updated. The final registered MRI is selected by the highest encountered image similarity value. In the following sections, each part of the workflow will be described in detail.

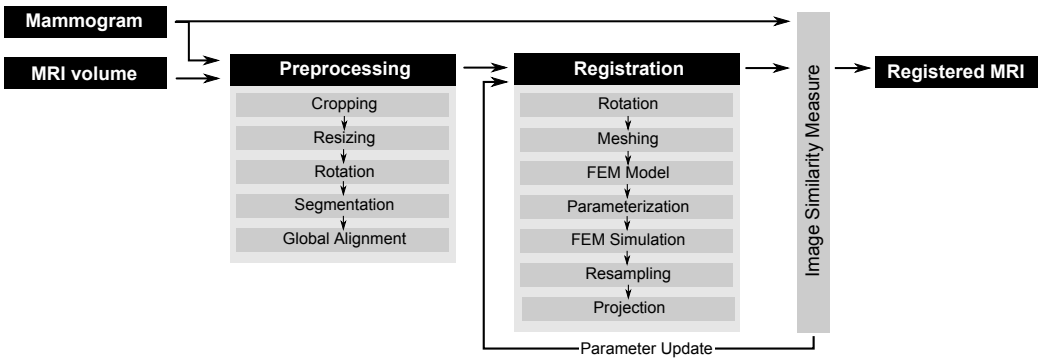

Figure 1: Workflow of the image registration.

2.1. Preprocessing

X-ray mammograms as well as MRI volumes have to be preprocessed. The MRI volume is cropped, i.e. the left or right breast is selected. Afterwards the cropped volume is rotated to fit the internally used coordinate system. A slice-based segmentation is carried out using thresholding, morphological operations and active contours (Chan and Vese, 2001). For a smooth surface in 3D, a smoothing of the segmentation mask by iterative Gaussian filtering is applied (Fang and Boas, 2009). To overcome gaps between the MRI slices, a linear interpolation between the slices is applied to obtain isotropic image resolution. More details on the preprocessing steps are presented in Hopp (2012).

The breast in the X-ray mammogram is segmented and rotated according to the MRI preprocessing. Downscaling is performed using a linear interpolation in order to meet the resolution of the MRI volume.

The volume of imaged tissue in both modalities varies considerably. In order to register the images, the tissue volume has to be matched. Our automated approach approximates the breast volume shown in the preprocessed

MRI volume by the number of all non-background voxels. The volume of the tissue imaged in the X-ray mammogram is obtained via an approximation of the breast by a semi-ellipsoid. The diameters are estimated from the segmented non-background area and the measured thickness of the breast in the compressed state, which is known from the mammogram's metadata. The MRI volume respectively the mammogram is cropped iteratively by one voxel in anteroposterior direction until the difference between both estimated volumes becomes minimal. In case of an unrecorded compression thickness in the mammogram's metadata, the compression thickness could be estimated as the free parameter of the semi-ellipsoidal approximation assuming equal amount of imaged tissue in both modalities (Ruiter et al., 2006).

For a first rigid alignment of the images, the cropping position in anteroposterior direction is used as reference, i.e. the posterior-most boundaries of the cropped MRI volume and the X-ray mammogram are mapped on each other. The rigid alignment in mediolateral direction is afterwards determined by translating the projection of the MRI volume over the mammogram. At maximally overlapping areas of the projected volume and the X-ray mammogram, the final aligned position is found.

2.2. Construction of Biomechanical Model

To simulate the compression applied to the breast during mammography, a biomechanical model is generated on the basis of the preprocessed MRI volume. FEM (Zienkiewidz and Taylor, 2000a,b) is used to emulate the physical behavior of the breast during the deformation process. The simplified principle of the registration process is illustrated in Figure 2.

The geometry of the biomechanical model is described by a tetrahedral

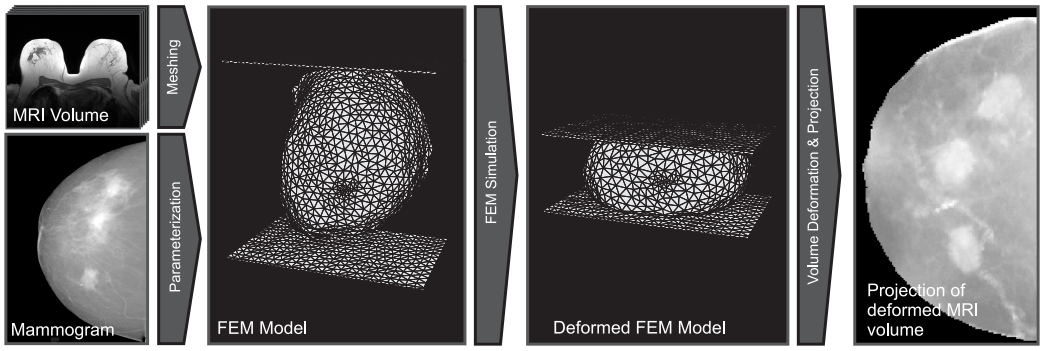

Figure 2: Simplified principle of the registration process.

mesh with an average of approximately 25,700 elements. It is generated using a MATLAB meshing algorithm (Fang and Boas, 2009) based on TetGen (Si, 2006). In order to distinguish between tissue types, the MRI volume is classified into voxels, representing fatty and fibroglandular tissue via thresholding, morphological operations and three-dimensional smoothing. For each finite element (FE), the type of tissue is assigned using a majority decision of voxels representing fat respectively gland within the element.

The physical behavior is described by the material model and boundary conditions of the compression simulation. Obtaining automatically the true material properties for each dataset is not feasible due to the qualitative imaging by MRI. Therefore the material is modeled constant for all patients. The stress-strain relationship of the breast tissue is described by a hyperelastic Neo-Hookean material model with material parameters defined by Wellman et al. (1999). In a previous study (Hopp and Ruiter, 2011), the stiffness ratio between fatty and glandular tissue was evaluated and optimized for our method. Glandular tissue is modeled with a 7.5 times higher Young's modulus than fatty tissue. Accordingly the Poisson's ratio

was optimized in a previous study (Hopp, 2012). The registration process was carried out with three datasets and the registration accuracy was evaluated. The median best result was obtained with a Poisson's ratio of 0.3. This value was therefore applied in the present study. Due to the unknown patient-individual anisotropic behavior (e.g. caused by Cooper's ligaments), tissues are assumed to be isotropic. Although tumors have a higher stiffness than fatty and glandular tissue (Wellman et al., 1999), the stiffness of tumors is not modeled introducing no a-priori knowledge into the simulation. Nodes of the FE mesh at the back are kept in position in anteroposterior direction to model the fixation of the breast at the chest wall.

2.3. Deformation Simulation

The deformation simulation is carried out using the commercial FEM software package Abaqus (Dassault Systèmes, 2011). The mammographic compression is mimicked by a two-step approach. In the first step (Figure 2), compression plates are added to the simulation, which are moved closer until the thickness of the breast during mammography is reached. The contact between compression plate and breast surface is assumed to have a high friction, i.e. the breast does not undergo a large sliding on the surface of the compression plate. In Abaqus a small-sliding interface can be used to approximate the behavior. It allows only small relative sliding between neighboring nodes on both surfaces. The contacting nodes are pre-calculated, which allows for a fast computation (Dassault Systèmes, 2009). The small-sliding interface therefore approximates a high friction coefficient while the computation can be carried out efficiently and convergence problems by explicitly restricting nodes from undergoing a friction via boundary condition defini-

tion are avoided. Due to the large necessary compression, Abaqus utilizes small-step incremental methods to solve the non-linear equation system numerically.

Usually, circumferences of the deformed MRI volume and the X-ray mammogram do not overlap completely at this stage. This is due to uncertainties and simplifications of the biomechanical model. For example, supporting structures of the breast (i.e. Cooper's ligaments) are not modeled as they are not depicted in the MRI. Frequently these simplifications result in a lower mediolateral expansion than could be observed in real mammograms (Tanner et al., 2009; Ruiter et al., 2006).

These deviations are compensated by the second simulation step. A three-dimensional model of the deformed configuration of the breast is approximated based on the mammogram. Different from the simple model to estimate the amount of tissue in both modalities, the circumference of the segmented mammogram is used as ground truth to be achieved by a projection image of the deformed MRI. Due to the projection acquisition, the real shape of the breast in 3D during mammography acquisition, i.e. the shape of the breast tissue in craniocaudal direction between the compression plates, is lost and therefore has to be estimated. In our 3D model this shape is approximated semi-ellipsoidally. For more details on the construction of this model refer to Hopp et al. (2012a) and Hopp (2012). The model is sampled in the resolution of the MRI volume. This three-dimensional model is named target model throughout this paper.

The target model is compared to the deformed MRI volume derived from the first simulation step. Displacement vectors between surface nodes of

the FEM mesh and the target model are defined on nearest neighbor basis. These displacements are used to describe new boundary conditions for the second simulation step. It results in a configuration of the MRI volume that is directly comparable to the mammogram since a projection image of the deformed MRI volume shows overlaying circumferences with the mammogram. To create projection images of the deformed MRI, a parallel projection is applied.

Both simulation steps are carried out using the MRI volume that was acquired before contrast agent injection. The simulated deformation field can be applied to all acquired MRI volumes of the same patient after contrast agent injection. We assume that the MRI protocol provides a pre-registration of MRI volumes for motion artifact suppression.

2.4. Intensity Based Optimization

The whole registration process depends on a number of parameters that influence the registration accuracy. In order to adapt the registration process to patient-specific conditions, an intensity-based optimization of parameters via image similarity measures is used.

In previous studies (Hopp and Ruiter, 2011; Hopp, 2012) we evaluated the effect of several relevant parameters on the registration accuracy. We found out that the cropping position of the MRI in anteroposterior direction and the rotation around the anteroposterior axis (the so-called "breast rolling") causes the highest variance in registration accuracy. While we can compensate for the cropping quite satisfactory by using our tissue matching algorithm presented in section 2.1, the possible rotation of the breast was not considered. Hence, in this study we apply an optimization of the rotation

parameter.

Rotation around the anteroposterior axis is applied to the MRI volume before registration. Afterwards, image similarity is calculated between the aligned projection image of the deformed MRI volume and the mammogram.

In the formal notation, the similarity metric is denoted as $\mathbf{S}$. The registration $\mathbf{R}$ uses a parameter set $\vec{p}$ to carry out the processing steps described before. $\mathbf{S}$ is used as optimization criterion. $\mathbf{R}(\vec{p})$ obtaining $\mathbf{S}_{max}$ provides the final registration result:

$$\vec{p}_{S_{max}} = \arg\max\left(\mathbf{S}\left(\mathbf{R}\left(\vec{p}\right)\right)\right). \tag{1}$$

As a result of different physical parameters imaged in both modalities, tissue is represented differently. We compensate this by combining MRI volumes acquired before (pre-contrast series) and after (post-contrast series) contrast agent injection as well as a subtraction of these series. Additionally a segmented MRI volume showing mostly glandular structures is used. The automatic segmentation of glandular structures was carried out by relative thresholding, morphological operations and a three-dimensional smoothing.

The combination of images is carried out by calculating a weighted pixelwise sum of aligned projection images of the considered deformed volumes. Additionally, gamma correction and median filtering are applied. This yields a projection image of the deformed MRI volume with comparable structures as the mammogram.

To optimize the weighting factors, a registration without rotation of the datasets was carried out for all available datasets. Afterwards Normalized Mutual Information (NMI) between the mammogram and the combined im-

age was calculated. The weighting factors with the highest average of the NMI values were then considered to be optimal and used for intensity-based optimization of the rotation parameter. Details on these experiments and the obtained results will be given in section 3.1.

2.5. Evaluated Data

Solely datasets from clinical routine at University Hospital at Jena (Germany) were considered in the present study. Each dataset consists of a MRI study and the corresponding craniocaudal mammogram of the same patient. MRI studies include pre- and post-contrast series. Additionally, subtraction images are available. All MRI studies were acquired on 1.5 Tesla scanners (Magnetom Symphony, Sonata and Avanto, Siemens Medical, Erlangen, Germany) using dedicated bilateral breast coils with the patient in prone position and a standardized protocol, according to international guidelines. The MRI series used in the present work are dynamic T1-weighted spoiled gradient echo scans (matrix size $= 384 \times 384$, slices $= 33$ - 44, in plane resolution $= 0.9 \times 0.9$ mm, slice thickness $= 3$ - 4 mm depending on scanner parameter choice, Field of view $= 350$ mm, time of acquisition $= 1$ min per measurement, time of repetition (TR) $= 113$ ms, echo time (TE) $= 5$ ms). As contrast agent, 0.1 mmol/kg bodyweight gadopentetate-dimeglumine (Gd-DTPA, Magnevist, Bayer HealthCare, Leverkusen, Germany) was administered at 3 ml per second intravenously, using a power injector (Medrad, Spectris, Pittsburgh, USA) for standardized injection. The contrast agent injection bolus was followed by 20 ml of physiological saline solution. After a delay of 30 s from the beginning of the contrast agent injection, DCE-MRI was carried out seven times with the same parameters. X-ray mammograms

used in the present work are acquired digitally on a Senograph 2000D or a Hologic Lorad Selenia full-field digital mammography system.

Considered datasets had to show at least one clearly visible lesion in both, the MRI and mammogram, for evaluation purposes. The lesion had to be included within the breast volume imaged in the MRI breast coil. Patients with mastectomy or changes in breast shape due to surgery were excluded. Only datasets with a known thickness of the breast during mammography, i.e. present in the DICOM header, were considered.

2.6. Evaluation Metric

To evaluate the accuracy of the registration, the target registration error (TRE) of landmarks is calculated. For each dataset used in this work, a lesion that is visible in both modalities, was marked by two experienced radiologists in consensus. The circumference of the lesion in the MRI volume is defined by six points, representing the maximal expansion of the lesion in each direction. The center point was calculated as the arithmetic average of these points. Accordingly within the mammogram, four points representing the maximal expansion of the lesion in each direction were acquired and stored in a database. The lesion position is approximated for the MRI by a cuboidal respectively for the mammogram a rectangular bounding box. The point locations of the markings in the MRI volumes were transformed according to the simulated deformation.

To calculate the TRE, the displacement of the projected center of the lesion marked in the MRI (C_{MRI}) and the lesion marked in the mammogram (C_{XR}) is measured as the Euclidean distance in the aligned projection images:

$$\mathrm{TRE} = ||C_{XR} - C_{MRI}|| \,. \tag{2}$$

The overlap of lesion markings is calculated as percentage of the overlapping pixels of the rectangle surrounding the lesion. Furthermore, we introduced a relative accuracy measure, which takes into account that the subjective perception of accuracy depends on the size of the lesion: e.g. for small lesions it is more important to have a small TRE. The relative accuracy measure TRE_{rel} is defined as the TRE divided by the diameter of the lesion in the mammogram D_{XR}:

$$\mathrm{TRE}_{rel} = \frac{\mathrm{TRE}}{D_{XR}}. \tag{3}$$

All registration results with $\mathrm{TRE}_{rel} \leq 1$ are considered as good registration results. In such cases – assuming an approximately equal size of the lesion markings in the mammogram and the MRI volume – the lesion markings overlap.

3. Results

79 datasets of 78 patients from clinical routine were included in the present study. All images were acquired using the parameters described in section 2.5. The mean volume of the breast was $0.75\,l$ (range 0.12 - $1.40\,l$). 83 lesions were marked by experts within the datasets to estimate the registration accuracy. The mean age of patients was 59 years (range 24 - 82 years). The mean diameter of the lesion markings was 25.8 mm (SD: 17.8 mm) within a projection of the MRI volume along the mammographic projection axis.

Within the mammograms the mean diameter was 23.6 mm (SD: 15.8 mm). The average difference of the size of markings was 6.2 mm.

3.1. Composition of MRI Projection Image

In a first step the registration of the 79 datasets was carried out without using the intensity-based optimization. For image comparison by an image similarity measure, we proposed a combination of pre- and post-contrast series as well as subtraction MRI volumes using a weighted sum. The aim was to achieve a projection image of the deformed MRI volume with comparable tissue structures to the mammogram.

Based on the first registrations, the weighting factors for the image composition were optimized. For all datasets the NMI value between the combined image and the X-ray mammogram was calculated. The weighting factors of the five different MRI volumes (Fig. 3 a) - e)) were varied in a range of 0 to 2. Additionally the median filter size and the gamma correction value were varied. The highest mean NMI over all datasets was found for an equal weight of gland-segmented pre-contrast series and the summation projection of the subtraction series filtered by a 5×5 median filter (Lim, 1990) without any gamma correction (Fig. 3 f)).

3.2. Evaluation of Registration Accuracy

Only using an alignment of datasets at the chest wall without registration, the mean TRE was 26.0 mm. Image registration was carried out, according to the method described in the previous section. The mean mammographic compression applied to the biomechanical models was 46.6 % (range 27.6 % - 74.6 %).

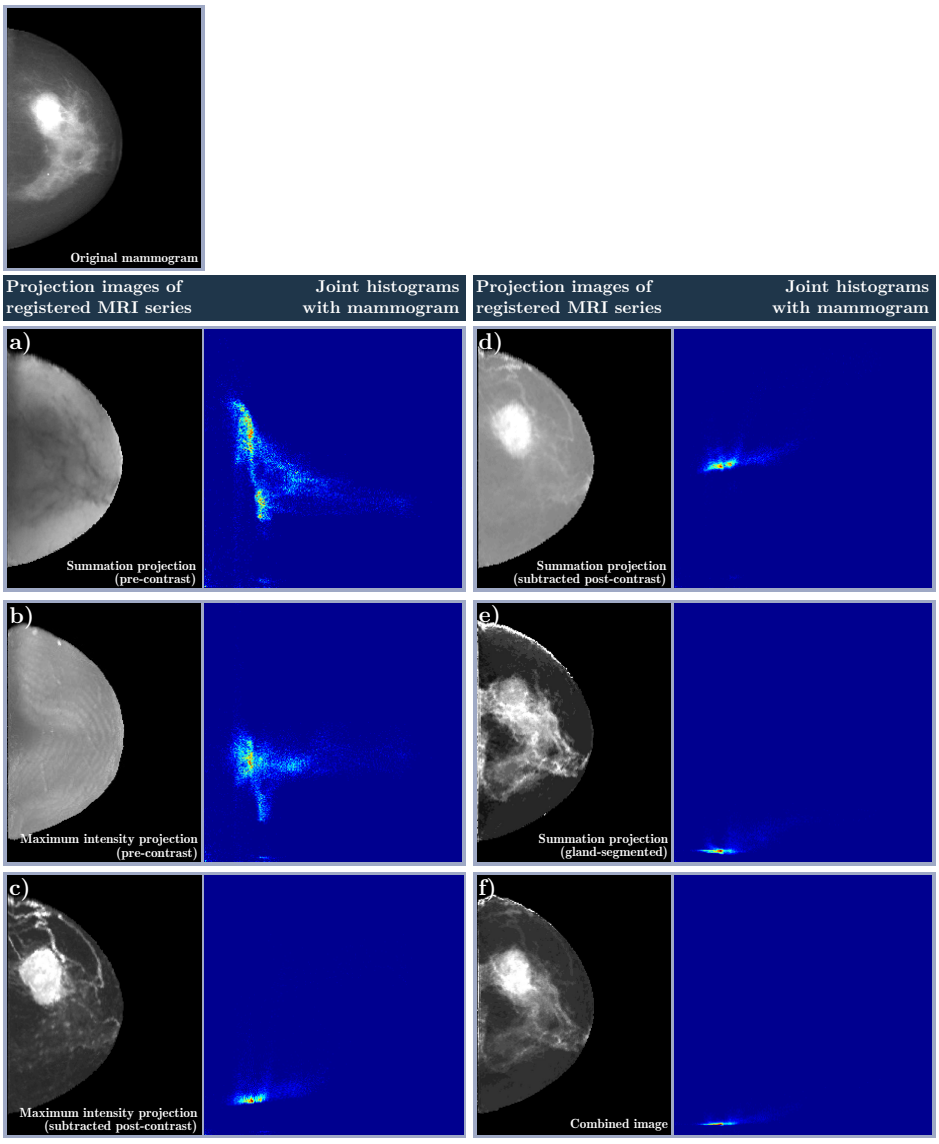

Figure 3: Composition of projection images for image similarity calculation. From a) to d): summation and maximum intensity projections of the pre-contrast series and the subtraction of the pre- and post-contrast series, e): projection of a volume with segmented glandular tissue, f): final combined image. For each projection image, the joint histogram with the X-ray mammogram (top) is given.

By performing the compression plate simulation, the mean TRE is reduced to 19.4 mm.

After performing the target model simulation, the mean TRE was 14.3 mm.

In order to evaluate the performance of the automatic cropping, the displacement of the lesion centers was examined in each direction. We detected a mean displacement of 7.2 mm in anteroposterior direction against a mean displacement of 10.8 mm in mediolateral direction. Hence, dataset rotation that tries to compensate the displacement in mediolateral direction was expected to decrease the mean TRE.

We applied a rotation between -15° to 15° in steps of 5°. By choosing the rotation angle which delivers minimal TRE for each dataset, the mean TRE can be reduced to 11.0 mm. However finding the minimal TRE for each dataset in this fashion involves prior knowledge about the lesion positions. In absence of known lesion positions, we determine the best rotation angle by our image similarity approach.

When performing our fully automated registration using image similarity measures and the optimized combined images to determine the rotation angle, mean TRE was reduced to 13.2 mm, the mean overlap of markings was 60 %. TRE_{rel} showed a mean value of 0.88. 57 datasets (72 %) had a TRE_{rel} below 1, hence delivered a good registration result with an overlap of lesions. 35 datasets (44 %) obtained a TRE better than 10 mm, 51 datasets (65 %) reached a TRE better than 15 mm. The TRE was reduced by a factor of two compared to the unregistered datasets. The mean displacement of the lesion markings in mediolateral direction without and respectively with rotation optimization was reduced from 10.8 mm to 9.7 mm. The image similarity

	TRE			**TRE$_{rel}$**			**Overlap**		
	mean	median	SD	mean	median	SD	mean	median	SD
Rigid alignment	26.0 mm	23.3 mm	13.4 mm	1.53	1.24	1.24	15 %	0 %	22 %
Alignment after compression plate simulation	19.4 mm	16.3 mm	11.5 mm	1.23	0.81	1.13	34 %	25 %	35 %
Registration without rotation optimization	14.3 mm	11.6 mm	9.6 mm	0.96	0.60	1.07	56 %	64 %	40 %
Registration with best choice of rotation	11.0 mm	8.3 mm	8.5 mm	0.73	0.38	0.90	69 %	88 %	37 %
Registration with automatic intensity-based rotation optimization	13.2 mm	11.5 mm	9.3 mm	0.88	0.56	1.0	60 %	75 %	40 %

Table 1: Summary of resulting registration accuracies (mean, median and standard deviation (SD)) for different registration methods.

Projection image type of registered MRI series	Mean TRE
Summation projection (pre-contrast)	13.9 mm
MIP (pre-contrast)	14.7 mm
MIP (subtracted post-contrast)	14.3 mm
Summation projection (subtracted post-contrast)	13.8 mm
Summation projection (gland-segmented)	13.6 mm
Optimized combined image	13.2 mm

Table 2: Results of the intensity-based optimization using different projection image of the registered MRI series.

measure used to carry out the intensity-based optimization was NMI.

Resulting images are shown in Figure 4. Table 1 summarizes the given results.

To evaluate the improvement of the intensity-based optimization by the proposed optimized combination of MRI series, the presented results were compared to registration runs using intensity-based optimization, but only the single MRI series (see Fig 3) to calculate image similarity. The results of this evaluation are given in Table 2.

3.3. Analysis of Datasets

In a next step we analyzed datasets in order to predict the registration accuracy that can be expected before starting the registration. 60 features were automatically extracted from the original datasets, e.g. the position of the nipple in MRI and mammogram, the amount of compression applied and the position and the size of the lesion. The ranges of the feature values were normalized to values between 0 and 1. The correlation coefficient of

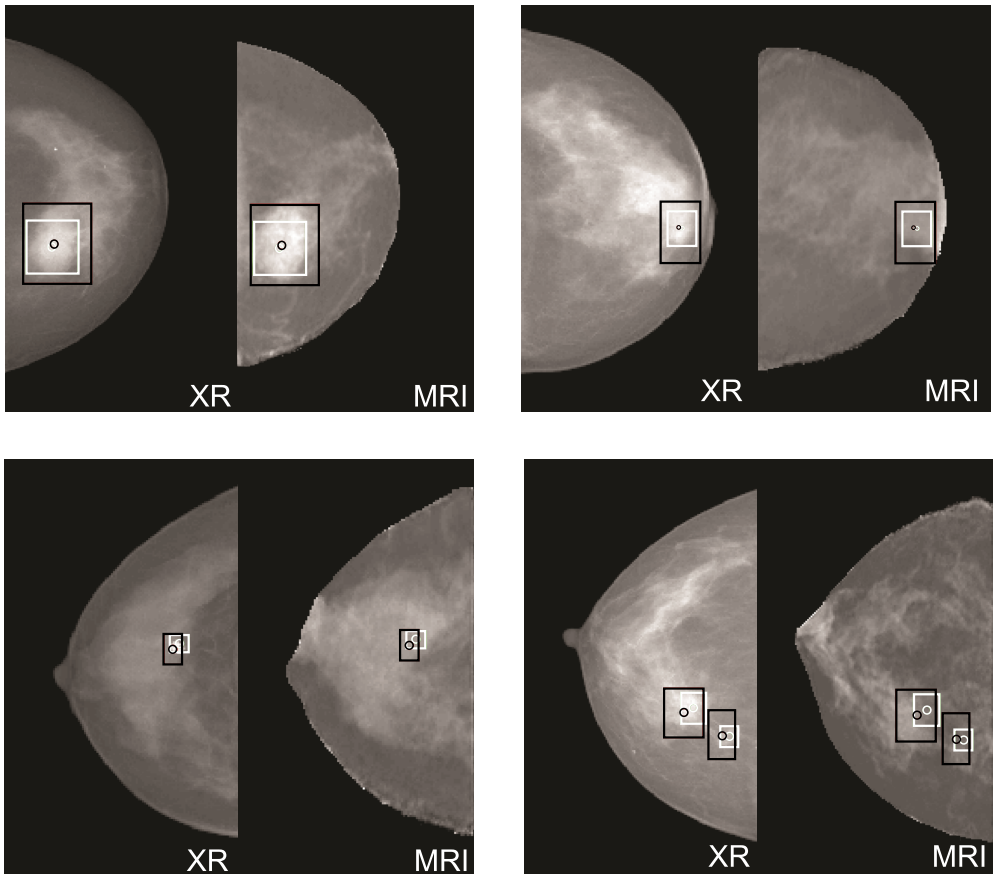

Figure 4: Registration results of four patients: mammogram (left) and projection of registered MRI (right). The lesion marking is represented by a white rectangle (mammogram annotation) respectively a black rectangle (MRI annotation).

each feature and the TRE was calculated. Afterwards, most contributing features were selected and combined using a forward-selection. The maximal correlation coefficient of the combined features with the TRE was 0.73. It was reached by combination of the ten most contributing features. Four of these ten features were related to the lesion position in the MRI volume and the X-ray mammogram. Furthermore, two features were related to the deviation of the nipple in the MRI volume from an ideal position. The correlation analysis with all features is referred to as "full feature set".

In the general application of our method, the information about the lesion position is mostly not present. In consequence features related to the lesion position cannot be calculated. By leaving out such features (referred to as "reduced feature set"), the maximal correlation coefficient was 0.52 using a combination of three features. The features include the size change of the breast in anteroposterior direction during the target model simulation and two features concerned with the nipple deviation from an ideal position in the MRI volume.

Figure 5 shows a scatter plot of the TRE against the combined and normalized feature values for the full feature set. Each point represents a registered dataset. Vertical dotted lines represent an exemplary partitioning of datasets into three categories. Table 3 illustrates the mean TRE for each category. For the reduced feature set, the partitioning into three categories using the same limits as illustrated in Table 3 yields a mean TRE of 10.3 mm for category A (63% of datasets included), 16.5 mm for category B (32%) and 30.2 mm for category C (5%).

To account for a possible overfitting, training sets (90% of the datasets)

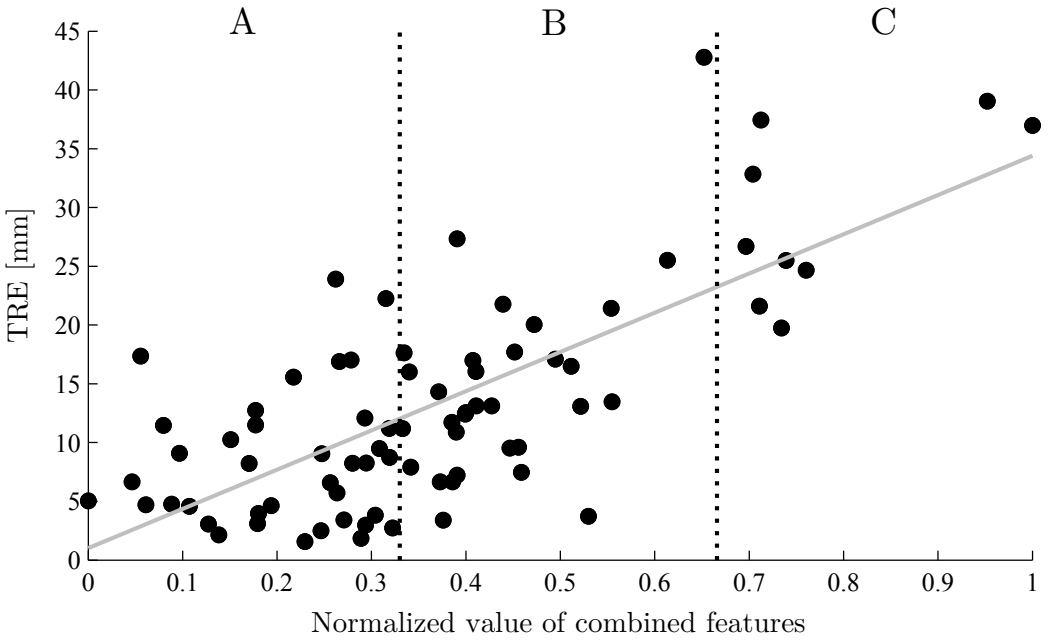

Figure 5: Scatter plot showing the TRE against a combination of ten features extracted from initial datasets (full feature set). The solid line represents the least-squares line. Vertical dotted lines represent an exemplary partitioning of datasets. The ranges A, B and C correspond to feature categories < 0.33, $0.33 - 0.66$ and > 0.66. The correlation coefficient was 0.73.

	Category A	**Category B**	**Category C**
Feature values	≤0.33	0.33 - 0.66	>0.66
Number of datasets	38 (48 %)	32 (41 %)	9 (11 %)
Mean TRE	8.4 mm	14.5 mm	29.4 mm
Median TRE	7.4 mm	13.1 mm	26.7 mm
SD TRE	5.7 mm	7.8 mm	7.3 mm

Table 3: Exemplary partitioning of datasets into three groups by a combination of ten features from the full feature set.

were selected randomly. For the according test set cases, the measured TRE was compared to the predicted TRE, which was obtained by the least squares fit. For 1000 repetitions of the training set selection, the mean distance between both values was 6.3 mm for the full feature set respectively 6.8 mm for the reduced feature set. A dataset for which the real TRE was higher than the predicted TRE plus the SD of the predicted category was defined as a misclassification. For 1000 repetitions, an average of 13% (full feature set) respectively 13% (reduced feature set) of misclassifications were observed.

3.4. Prediction of Registration Accuracy

Based on the extracted features, we classified the datasets into categories which represent a good registration accuracy below a TRE of 15 mm respectively a suboptimal registration accuracy with a TRE above 15 mm. Experiments were done using the data mining tool WEKA (Hall et al., 2009). A best-first selection of parameters was carried out using a 10-fold cross-

validation. Five features were selected and passed to a J48 tree classifier[5]. 10-fold cross-validation was used to evaluate the performance of the classifier. The results showed 85 % correctly classified datasets with a sensitivity of 90 % and a specificity of 75 %.

4. Discussion

In this paper we presented a fully-automated approach for registration of X-ray mammograms with DCE-MRI volumes. The registration works for images from clinical routine without the need for user interaction. Though the clinical variability of datasets is large, the accuracy shows promising results with a mean TRE of 13.2 mm. The obtained results are in the same range as the accuracies achieved in literature though in this work a fully automated approach was used. Most approaches in literature require at least some manual interactions (Mertzanidou et al., 2012) respectively optimizations (Lee et al., 2011). A considerably higher number of datasets than in our earlier publications (Hopp et al., 2012a; Dietzel et al., 2011) improves statistical robustness. Only craniocaudal mammograms have been considered in the present study. However, the method can be extended to handle oblique mammograms (Hopp and Ruiter, 2012) similar to Ruiter et al. (2006).

The datasets used in this study were acquired with a standardized protocol, according to international guidelines. However, the registration is not limited to this acquisition protocol. Our method is able to register images from different volumetric modalities with X-ray mammograms. It was also

[5]The J48 tree classifier is an implementation of the C4.5 algorithm proposed by Quinlan (1993).

tested with 3.0 Tesla MRI images and Ultrasound Computer Tomography images in previous studies (Dietzel et al., 2011; Hopp et al., 2011), achieving a registration accuracy in the same range as in the present study. Only the preprocessing - i.e. automatic cropping of datasets, segmentation and rotation to internal coordinate system - has to be adapted to the modality specific conditions.

The registration does not take gravity into account. This is motivated by earlier studies (Ruiter et al., 2006; Rajagopal et al., 2010) reporting insignificant influence of gravity in simulation compared to mammographic compression. Also tumor stiffness is not modeled which may result in a change of the lesion size in the projection image by compressing the MRI volume. However, different types of tumors are likely to vary in stiffness (Wellman et al., 1999; Krouskop et al., 1998; Samani et al., 2007). Hence, the tumor type would need to be taken into account when modeling tumor stiffness explicitly. This would result in the need for a user interaction or a highly complex and accurate computer assisted detection process and diagnosis. In contrast, our model uses no a-priori knowledge for modeling. This also holds for neglecting an exact modeling of the chest wall according to previous evaluations indicating a marginal effect by including a more complex model (Hopp and Ruiter, 2011).

The simulation of the mammographic compression is carried out in two steps. In the first simulation step, the main breast compression is simulated. The biomechanical model used in this work is a simplification of the real breast since there exist several uncertainties about the real mechanical behavior and not all tissue structures in the breast are depicted in the

underlying images. The second simulation therefore compensates for these simplifications by applying surface displacement boundary conditions to align the circumferences of the images.

The low Poisson's ratio used in this work was evaluated in a previous study (Hopp, 2012) by a parameter optimization using a subset of the datasets. While the low Poisson's ratio partly disagrees with the assumption of volume preservation, the use of this lower value contributes to less expansion in anteroposterior direction, i.e. the shape of the breast in anteroposterior direction is already similar to the circumference of the mammogram. The macroscopic anisotropy (Tanner et al., 2009; Ruiter et al., 2006) of the breast is compensated using the target model simulation afterwards. In this step mainly the mediolateral expansion needs to be corrected. The volume of the breast is approximately preserved by applying the target model simulation step. The volumes were evaluated by counting all non-background voxels in the image before and after registration. After registration, the volume was in average increased by approximately 13% compared to the unregistered dataset. This increase may partly be caused by interpolation artifacts which occure at the breast boundaries when deforming the volume image.

In earlier work (Hopp and Ruiter, 2011; Hopp, 2012) we found out that datasets from clinical routine can vary considerably in the acquisition procedure, e.g. positioning of the breast during mammography or MRI and breast shape. As a first patient-specific optimization, we compensated for breast rolling. The optimization of dataset rotation, using image similarity measures, improved the mean registration accuracy by approximately 1.1 mm. It has to be considered that e.g. for central lesions a rotation of datasets

is less effective than for lateral lesions. Also we found datasets for which a rotation by an angle above 15° could possibly improve the registration accuracy. In the particular case shown in Figure 6 (right), TRE can be reduced from 34 mm to 13 mm using a rotation angle of 20°. Therefore, allowing a increased computation time, the registration accuracy may be improved by considering a wider parameter range. A deeper evaluation with an extended parameter range along with a reduction of computation time is subject to our future work.

Furthermore, we found some cases in which the automatic cropping provided an overestimation of the mammogram volume (e.g. Figure 6 (left)). Consequently, the displacement of a lesion in anteroposterior direction is dominant. By different cropping, TRE can be reduced from 32 mm to 9 mm in the particular case. Our ongoing work focuses on the improvement of the tissue estimation for a more robust automatic cropping of datasets and reduction of anteroposterior registration error.

In a previous study, the effect of different parameterizations – e.g. the Poisson's ratio as described before – of the registration process was evaluated with one (Hopp and Ruiter, 2011) respectively three (Hopp, 2012) datasets due to limitations by the computation time. The resulting best parameters which gave the lowest TRE were applied as constant parameter set in the present work. Only the breast rotation was used as free parameter during the patient-specific optimization. However the method is to carry out the intensity-based optimization with an extended parameter space, i.e. also the parameters which were chosen to be constant in this study may be subject to a patient-specific optimization in future.

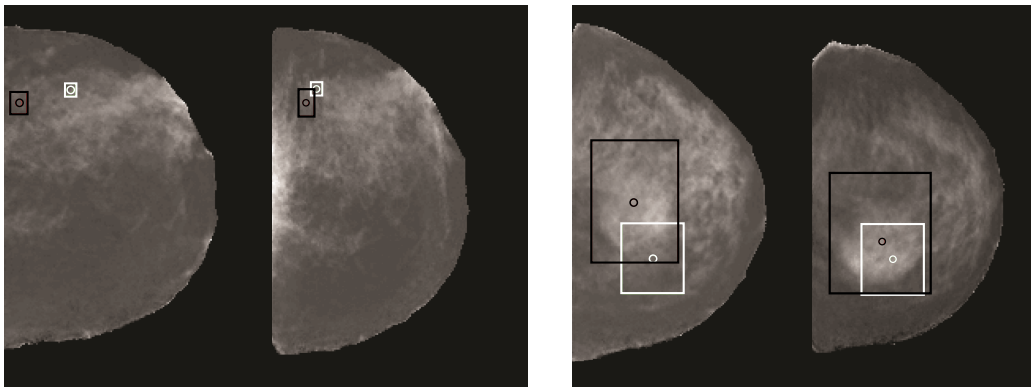

Figure 6: Registration results of two patients with suboptimal registration accuracy. Different cropping may decrease TRE (left). Rotation of dataset with more than 15° may decrease TRE (right).

The registration was tested with datasets displaying a lesion in both the mammogram and the MRI volume. Lesion marking was carried out by two experienced radiologists in consensus and used as ground truth for registration accuracy evaluation. As a result of different physical basis, lesions may be rendered differently in both modalities. Defining the exact borders of the lesions is a challenging task, even for experienced radiologist. Additionally the marking is time consuming. Therefore lesions were acquired by setting a bounding box around the lesion. The given registration accuracy can be seen as an approximation and all given accuracy measures should be regarded together for interpretation of the results. Due to the absence of standard measures, the given values, however, provide an estimation of the quality of the method.

Lesion positions were not used as landmarks for registration. Our patient set included a large variety of lesions, either in size, location or contrast

enhancement. Image similarity based optimization seems not to be influenced by the nature of the lesion. Also in cases where no contrast enhancement was identified, the optimization of the rotation angle worked well. This leads us to the conclusion that our registration approach does not strongly depend on the presence of a clearly visible lesion.

In order to optimize the registration patient-specifically using image similarity, presence of glandular structures in the images seems to be important. However the density of breasts varied considerably throughout the considered datasets. There was no substantial influence of the breast density on the imaged-based optimization of the registration. Also for cases in which neither contrast-enhancement in the MRI nor detailed glandular structures in the X-ray mammogram (BIRADS I, density well below 15%) could be observed, the intensity-based optimization did not degrade the registration accuracy. Furthermore the target group of patients that can benefit from our method in clinical practice are particularly patients with dense breasts, e.g. with unclear findings in the mammogram due to superimposition of glandular structures.

By automatically extracting features from the original datasets, the registration accuracy can be estimated and datasets can be categorized in order to give additional information to the observing radiologist. The correlation between the features was carried out using a set of 60 features reaching a maximal correlation coefficient of 0.73. Though the maximal value decreases to 0.52 by leaving out lesion-related features, the correlation is still significant ($p < 0.005$). Therefore also with a limited feature set, the registration accuracy can be estimated. If additional information, e.g. the lesion position

in one modality, is available, it may be included to increase the significance.

Our current work focuses on a clinical evaluation of the registration. Currently, the registration software is implemented in MATLAB for rapid prototyping. The registration of a dataset with a fixed parameter set, i.e. without intensity-based optimization, takes approximately 20 min on a standard desktop computer. Using seven rotation steps for an intensity-based optimization, a total computation time of approximately 120 min is needed. For clinical use the definite workflow, i.e. the parameters to be optimized, has to be established. The registration can thereafter be speeded up by the use of parallelization, e.g. by graphical processing units. Appropriate visualization methods have been developed (Hopp et al., 2012a). Additionally a interactive point localization in the alternative modality within our customized analysis software was implemented for the use in further studies (Hopp et al., 2012b). The analysis of a new dataset to be registered allows categorization by extraction of features. Thus, before registering the new dataset, the registration accuracy category of the dataset can be estimated. Accordingly, a safety margin may be presented to the radiologist.

5. Conclusion

For the first time, an image similarity based optimization of a FEM-driven 2D/3D breast image registration was evaluated with a large number of clinical datasets. Based on our evaluation, we conclude that a completely automated registration of volume images with 2D mammograms is feasible. The registration accuracy is within a clinically relevant range. Therefore we expect the combination of X-ray mammograms and MRI volumes in an

intuitive combined reading to benefit radiological diagnosis. Especially for patients with dense breasts, the correlation of information from two complementary modalities could be essential for a more accurate diagnosis. Because of the use of clinical standard modalities, no additional examination and image acquisition has to be performed.

References

American Cancer Society, 2011. Breast cancer facts and figures 2011 - 2012. Atlanta: American Cancer Society, Inc.

Baltzer, P., Dietzel, M., Vag, T., S.Berger, Freiberg, C., Herzog, A., Gajda, M., Camara, O., Kaiser, W., 2009. Can color-coded parametric maps improve dynamic enhancement pattern analysis in MR mammography? RoFo: Fortschr Geb Rontgenstr Neuen Bildgeb Verfahr 182, 254 – 260.

Behrenbruch, C.P., Marias, K., Armitage, P.A., Yam, M., Moore, N., English, R.E., Clarke, J., Brady, M., 2003. Fusion of contrast-enhanced breast MR and mammographic imaging data. Med Image Anal 7, 311 – 340.

Chan, T., Vese, L., 2001. Active contours without edges. IEEE Trans Image Proc 10, 266 – 277.

Chung, J.H., Rajagopal, V., Nielsen, P.M.F., Nash, M.P., 2008. A biomechanical model of mammographic compressions. Biomech Model Mechanobiol 7, 43 – 52.

Dassault Systèmes, 2009. Abaqus Theory Manual. V 6.9.

Dassault Systèmes, 2011. Abaqus 6.11 Online Documentation.

DeMartini, W., Lehman, C., 2008. A review of current evidence-based clinical applications for breast magnetic resonance imaging. Top Magn Reson Imaging 19, 143 – 150.

Dietzel, M., Hopp, T., Ruiter, N., Zoubi, R., Runnebaum, I.B., Kaiser, W.A., Baltzer, P.A., 2011. Fusion of dynamic contrast-enhanced magnetic resonance mammography at 3.0T with X-ray mammograms: Pilot study evaluation using dedicated semi-automatic registration software. EJR 79, 98 – 102.

Fang, Q., Boas, D., 2009. Tetrahedral mesh generation from volumetric binary and grayscale images, in: IEEE International Symposium on Biomedical Imaging: From Nano to Macro 2009, pp. 1142 – 1145.

Ferrant, M., Warfield, S.K., Nabavi, A., Jolesz, F.A., Kikinis, R., 2001. Registration of 3D intraoperative MR images of the brain using a finite element biomechanical model, in: IEEE Trans Med Imaging, pp. 1384 – 1397.

Fischer, T., Bick, U., Thomas, A., 2007. Mammographie-Screening in Deutschland. Visions J 15, 62 – 67.

Hall, M., Frank, E., Holmes, G., Pfahringer, B., Reutemann, P., Witten, I.H., 2009. The WEKA data mining software: An update. SIGKDD Explorations 11, 10 – 18.

Hopp, T., 2012. Multimodal Registration of X-Ray Mammograms with 3D Volume Datasets. Ph.D. thesis. University of Mannheim.

Hopp, T., Baltzer, P., Dietzel, M., Kaiser, W., Ruiter, N., 2012a. 2D/3D image fusion of X-ray mammograms with breast MRI: visualizing dynamic

contrast enhancement in mammograms. Int J Comp Assist Radiol Surg 7, 339–348.

Hopp, T., Bonn, J., Ruiter, N.V., Sak, M., Duric, N., 2011. 2D/3D image fusion of X-ray mammograms with speed of sound images: Evaluation and visualization, in: Proceedings SPIE Medical Imaging, p. 79680L.

Hopp, T., Ruiter, N., 2011. Configurable framework for automatic multimodal 2D/3D registration of volume datasets with X-ray mammograms, in: Proceedings of the Workshop on Breast Image Analysis in conjunction with MICCAI 2011, pp. 145 – 152.

Hopp, T., Ruiter, N., 2012. 2D/3D Registration for Localization of Mammographically Depicted Lesions in Breast MRI, in: Maidment, A., Bakic, P., Gavenonis, S. (Eds.), Breast Imaging, Springer Berlin Heidelberg. pp. 627–634.

Hopp, T., Ruiter, N., M.Dietzel, Kaiser, W., Baltzer, P., 2012b. Entwicklung und Test einer Open Source-basierten Software Infrastruktur für die strukturierte Befundung und Dokumentation im Rahmen multimodaler, multizentrischer radiologischer Studien, in: RöFo Fortschr Geb Rontgenstr Neuen Bildgeb Verfahr S1, Abstracts 93. Deutscher Röntgenkongress.

Houssami, N., Ciatto, S., Macaskill, P., Lord, S.J., Warren, R.M., Dixon, J.M., Irwig, L., 2008. Accuracy and surgical impact of magnetic resonance imaging in breast cancer staging: Systematic review and meta-analysis in detection of multifocal and multicentric cancer. J Clin Oncol 26, 3248 – 3258.

Kaiser, W.A., Fischer, H., Vagner, J., Selig, M., 2000. Robotic system for biopsy and therapy of breast lesions in a high-field whole-body magnetic resonance tomography unit. Invest Radiol 35, 513 – 519.

Kaiser, W.A., Zeitler, E., 1989. MR imaging of the breast: fast imaging sequences with and without Gd-DTPA. Preliminary observations. Radiology 170, 681 – 686.

Krouskop, T.A., Wheeler, T.M., Kallel, F., Garra, B.S., Hall, T., 1998. Elastic moduli of breast and prostate tissues under compression. Ultrason Imaging 20, 260 – 274.

Lee, A.W.C., Rajagopal, V., Reynolds, H.M., Doyle, A., Nielsen, P.M., Nash, M.P., 2011. Breast X-ray and MR image fusion using finite element modeling, in: Proceedings of the Workshop on Breast Image Analysis in conjunction with MICCAI 2011, pp. 129 – 136.

Lim, J.S., 1990. Two-dimensional signal and image processing. Prentice-Hall, Inc., Upper Saddle River, NJ, USA.

Martí, R., Zwiggelaar, R., Rubin, C.M.E., Denton, E.R.E., 2004. Two-dimensional - three-dimensional correspondence in mammography. Int J Cybern Sys 35, 85 – 105.

Mertzanidou, T., Hipwell, J., Cardoso, M.J., Zhang, X., Tanner, C., Ourselin, S., Bick, U., Huisman, H., Karssemeijer, N., Hawkes, D., 2012. MRI to X-ray mammography registration using a volume-preserving affine transformation. Med Image Anal 16, 966–975.

Mertzanidou, T., Hipwell, J., Han, L., Huisman, H., Karssemaijer, N., Hawkes, D., 2011. MRI to X-ray mammography registration using an ellipsoidal breast model and biomechanically simulated compressions, in: Proceedings of the Workshop on Breast Image Analysis in conjunction with MICCAI 2011, pp. 161 – 168.

Mertzanidou, T., Hipwell, J.H., Cardoso, M.J., Tanner, C., Ourselin, S., Hawkes, D.J., 2010. X-ray mammography - MRI registration using a volume-preserving affine transformation and an EM-MRF for breast tissue classification, in: Proceedings Digital Mammography / IWDM 2010, pp. 23 – 30.

Pisano, E.D., Hendrick, R.E., Yaffe, M.J., Baum, J.K., Acharyya, S., Cormack, J.B., Hanna, L.A., Conant, E.F., Fajardo, L.L., Bassett, L.W., D'Orsi, C.J., Jong, R.A., Rebner, M., Tosteson, A.N.A., Gatsonis, C.A., 2008. Diagnostic accuracy of digital versus film mammography: Exploratory analysis of selected population subgroups in DMIST1. Radiology 246, 376 – 383.

Quinlan, J.R., 1993. C4.5: programs for machine learning. Morgan Kaufmann Publishers Inc., San Francisco, CA, USA.

Rajagopal, V., Chung, J.H., Highnam, R.P., Warren, R., Nielsen, P.M., Nash, M.P., 2010. Mapping microcalcifications between 2D mammograms and 3D MRI using a biomechanical model of the breast, in: Comp Biomech Med, pp. 17 – 28.

Reynolds, H.M., Puthran, J., Doyle, A., Jones, W., Nielsen, P.M.F., Nash,

M.P., Rajagopal, V., 2011. Mapping breast cancer between clinical X-ray and MR images, in: Comp Biomech Med, pp. 81 – 90.

Ruiter, N.V., Stotzka, R., Mueller, T.O., Gemmeke, H., Reichenbach, J.R., Kaiser, W.A., 2006. Model-based registration of X-ray mammograms and MR images of the female breast. IEEE Trans Nucl Sci 53, 204 – 211.

Samani, A., Zubovits, J., Plewes, D., 2007. Elastic moduli of normal and pathological human breast tissues: An inversion-technique-based investigation of 169 samples. Phys Med Bio 52, 1565.

Schulz-Wendtland, R., Fuchsjäger, M., Wacker, T., Hermann, K.P., 2009. Digital mammography: An update. EJR 72, 258 – 265.

Si, H., 2006. TetGen. A Quality Tetrahedral Mesh Generator and Three-Dimensional Delauny Triangulator. Version 1.4. User's Manual.

Sivaramakrishna, R., Gordon, R., 1997. Detection of breast cancer at a smaller size can reduce the likelihood of metastatic spread: A quantitative analysis. Acad Radiol 4, 8 – 12.

Tanner, C., White, M., Guarino, S., Hall-Craggs, M., Douek, M., Hawkes, D., 2009. Anisotropic behaviour of breast tissue for large compressions, in: Biomedical Imaging: From Nano to Macro, 2009. ISBI '09. IEEE International Symposium on, pp. 1223 –1226.

Warner, E., Messersmith, H., Causer, P., Eisen, A., Shumak, R., Plewes, D., 2008. Systematic review: Using magnetic resonance imaging to screen women at high risk for breast cancer. Ann Intern Med 148, 671 – 679.

Wellman, P.S., Howe, R.D., Dalton, E., Kern, K.A., 1999. Breast Tissue Stiffness in Compression is Correlated to Histological Diagnosis. Technical Report. Harvard BioRobotics Laboratory.

Zienkiewidz, O., Taylor, R., 2000a. The Finite Element Method, Vol 1, 5th edition. Butterworth Heinemann, Oxford.

Zienkiewidz, O., Taylor, R., 2000b. The Finite Element Method, Vol 2, 5th edition. Butterworth Heinemann, Oxford.

Authors' biographies

T. Hopp

Torsten Hopp, Ph.D. was born in 1984 in Speyer. He studied computer science in Mannheim and Heidelberg. He received his M.Sc. degree in 2009 at the University of Heidelberg. Since 2003 he is working at the Institute for Data Processing and Electronics at Karlsruhe Institute of Technology. He has a Ph.D. degree (2012) in computer science from University of Mannheim, Germany. His research interests include digital image processing, medical imaging, image registration and biomechanical modeling.

M. Dietzel

Matthias Dietzel, MD was born in Erlangen. After training in several medical schools, including the University of Toronto and University of Zurich, he received his MD in 2006 at the Friedrich Schiller University Jena, Germany. He has been working in the breast MRI research group of the Friedrich

Schiller University Jena since 2004. Since 2012 is a radiologist at the University Hospital of Erlangen, Germany. His special interest includes clinical application of breast MRI, co-registration of X-ray and MR Mammogramms as well as application of breast MRI beyond local staging as a prognostic biomarkers.

P.A. Baltzer

Pascal Baltzer, MD was born in Cologne. He graduated and received his MD in 2005 at the Friedrich Schiller University Jena, Germany. He finished his residency at the Institute of Diagnostic and Interventional Radiology in 2011. He has been working in the breast MRI research group of the Friedrich Schiller University Jena since 2002. Currently he is a board certified radiologist at the Medical University of Vienna, Austria. His special interests include statistics and epidemiology in radiological research.

P. Kreisel

Peter Kreisel was born in Jena. He is currently a senior medical student at the medical school of the Friedrich Schiller University Jena, Germany. Peter has been working in the breast MRI research group of the Friedrich Schiller University Jena since 2009. His special interest is clinical application of image registration algorithms in breast imaging.

W.A. Kaiser

Prof. Werner A. Kaiser, MD was born in 1949 in Brühl. He studied chemistry and medical science in Karlsruhe and Freiburg. In 1975 he received his diploma in chemistry, in 1980 he earned his MD at the University of Freiburg.

In 1991 he promoted to professor at Rheinische Friedrich Wilhelms University Bonn. From 1993 to 1994 he held the chair at Institute for Diagnostic Radiology at University of Würzburg. Since 1994 he holds a professorship at the Friedrich Schiller University at Jena. Since 1994 he has been head of the Institute for Diagnostic and Interventional Radiology at University Jena. His major research activities include clinical application of breast MRI.

H. Gemmeke

Prof. Hartmut Gemmeke was born in Northeim in 1944. He studied exp. Physics in Goettingen and Heidelberg and received his Ph.D. degree from the University of Heidelberg in 1971. He joined Karlsruhe Institute of Technology in 1982. Since 1990, he has been a supernumerary professor at the University of Heidelberg and since 1996 at the University of Karlsruhe. Since 1993, he has been head of the Institute of Data Processing and Electronics at KIT. His present research activities are focused on embedded systems, data acquisition- systems, Ultrasound Computer Tomography and detection of air showers by their fluorescence and radio signals.

N.V. Ruiter

Nicole V. Ruiter, Ph.D was born in 1974. She has a M.Sc. degree (2000) in Medical Informatics from University of Heidelberg, Germany. She has a Ph.D. degree (2003) in Informatics from University of Mannheim, Germany. Currently she is with the Institute for Data Processing and Electronics at Karlsruhe Institute of Technology as scientist and project manager of the project Ultrasound Computer Tomography. Her research interests include

ultrasound imaging, image reconstruction, digital image and signal processing and biomechanical models.